A&A 457, 1071–1079 (2006)
DOI: 10.1051/0004-6361:20065227

Astronomy & Astrophysics

Fast magnetohydrodynamic waves in a two-slab coronal structure: collective behaviour

M. Luna, J. Terradas, R. Oliver, and J. L. Ballester

Departament de Física, Universitat de les Illes Balears, 07122 Palma de Mallorca, Spain
e-mail: [manuel.luna;jaume.terradas;ramon.oliver;dfsjlb0]@uib.es

Received 17 March 2006 / Accepted 12 July 2006

ABSTRACT

Aims. We study fast magnetohydrodynamic waves in a system of two coronal loops modeled as smoothed, dense plasma slabs in a uniform magnetic field. This allows us to analyse in a simple configuration the collective behaviour of the structure due to the interaction between the slabs.
Methods. We first calculate the normal modes of the system and find analytical expressions for the dispersion relation of the two-slab configuration. Next, we study the time-dependent problem of the excitation of slab oscillations by numerically solving the initial value problem. We investigate the behaviour of the system for several shapes of the initial disturbances.
Results. The symmetric mode respect to the centre of the structure is the only trapped mode for all distances between the slabs while the antisymmetric mode is leaky for small slab separations. Nevertheless, there is a wide range of slab separations for which the fundamental symmetric and antisymmetric trapped modes are allowed and have very close frequencies. These modes are excited according to the parity of the initial perturbation.
Conclusions. We find that for any initial disturbance the slabs oscillate with the normal modes of the coupled slab system, which are different from the modes of the individual slabs. We show that it is possible to excite the symmetric and antisymmetric trapped modes at the same time. This kind of excitation can produce the beating phenomenon, characterised by a continuous exchange of energy between the individual slabs.

Key words. Sun: corona – magnetohydrodynamics (MHD) – waves

1. Introduction

Transversal coronal loop oscillations are routinely observed by the EUV telescope on board *TRACE*. Several oscillating loops have been studied in detail by Aschwanden et al. (1999, 2002); Schrijver et al. (2002); Verwichte et al. (2004). Information about the period, damping time and amplitude of the oscillations has been derived. These kind of oscillations have been interpreted as standing kink fast magnetohydrodynamic (MHD) waves since they produce displacements of the loop axis and the loop footpoints seem to be anchored in the solar photosphere.

In general, the observed oscillating loops belong to complex active regions and in most cases they cannot be considered as isolated magnetic tubes. A clear example of such configurations are coronal arcades, where loops are located forming ensembles of several magnetic flux tubes. There is also observational evidence of transversal loop oscillations in such complex structures. For example, Verwichte et al. (2004), have studied in detail the features of the oscillating loops forming an arcade which were presumably disturbed by a prominence eruption. In fact, these observations suggest that the loops do not oscillate independently and that different loops oscillate following an organised motion.

From the theoretical point of view the behaviour of isolated magnetic structures have been studied in several geometries by Spruit (1981); Edwin & Roberts (1982, 1983); Cally (1986, 2003); Díaz (2004), little work has yet been done on multi-structures. Berton & Heyvaerts (1987) studied the magnetohydrodynamic normal modes of a periodic magnetic medium while Bogdan & Fox (1991) and Keppens et al. (1993) analysed the scattering and absorption of acoustic waves by bundles of magnetic flux tubes with sunspot properties. Murawski (1993); Murawski & Roberts (1994) studied the propagation of fast waves in two slabs unbounded in the longitudinal direction. On the other hand, the collective nature of oscillations has been investigated in multifibril Cartesian systems (see Díaz et al. 2005) representing the oscillation of the fibril structure of prominences. These authors found that in a system of equal fibrils the only non-leaky mode is the symmetric one, which means that all the fibrils oscillate in spatial phase with the same frequency.

Here we consider a simple line-tied two-slab model without gravity and curvature; and solve the time-dependent problem of the excitation of coronal loop oscillations. In general, an initial disturbance is likely to deposit some energy in the trapped modes, while some energy will be emitted via the leaky waves. We concentrate on the conditions that lead to the excitation of trapped and leaky modes and analyse in detail the behaviour of the system when more than a single trapped mode is excited at the same time. We compare the results of the time-dependent simulations with the information provided by the normal modes. This allows us to study the interaction between the oscillating slabs which leads to a collective behaviour of the system.

This paper is organised as follows. In Sect. 2 the loop model and the basic MHD equations describing fast waves are presented. In Sect. 3 the features of trapped and leaky modes are analysed in detail. In Sect. 4 the time-dependent problem is considered and the resulting velocity profiles are studied for

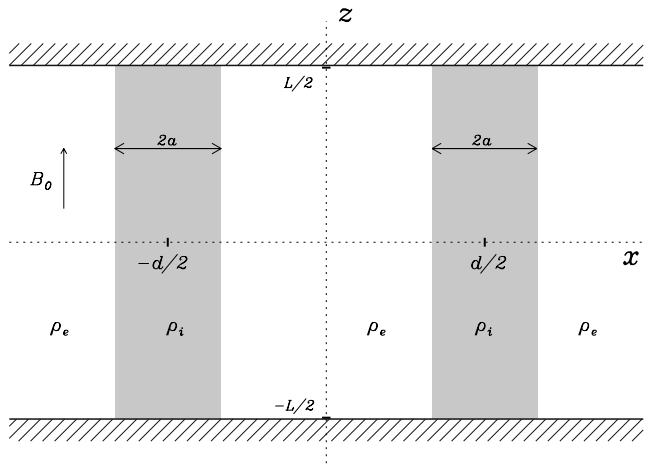

Fig. 1. Sketch of the two-slab system. The shaded area represents the density enhancement of the two slabs while the hatched area represents the photospheric medium, that fixes the feet of the slabs and produces the line-tying effect.

several initial perturbations. An analytical analysis of the beating is given in Sect. 5. Finally, in Sect. 6 the main conclusions are drawn.

2. Basic equations

We consider a system of two parallel loops modeled as dense plasma slabs of half-width a and length L (Fig. 1). The distance between the centres of the slabs is d, so the distance between their inner edges is $d - 2a$. The density profile is sharp and given by

$$\rho(x) = \begin{cases} \rho_{\rm e}, & \text{if } 0 \le |x| < d/2 - a, \\ \rho_{\rm i}, & \text{if } |x \pm d/2| \le a, \\ \rho_{\rm e}, & \text{if } |x| > d/2 + a, \end{cases} \tag{1}$$

where $\rho_{\rm i}$ and $\rho_{\rm e}$ are the density of the slabs and the coronal environment. The magnetic field is uniform and parallel to the z-axis, i.e. $\boldsymbol{B} = B_0\,\boldsymbol{e}_z$. For the sake of simplicity, gravity and curvature are neglected in the present model.

When considering perturbations about this equilibrium, we use the linearised magnetohydrodynamic (MHD) equations in the low-β limit ($\beta = 0$). In this limit the slow mode does not appear. To simplify the study of fast modes it is also assumed that perturbations do not depend on y, hence the Alfvén and fast modes are decoupled. Furthermore, we Fourier analyse in the z-direction, i.e. we assume that perturbations are of the form $\mathrm{e}^{-\mathrm{i}k_z z}$, which allows us to study the effect of photospheric line-tying by selecting the appropriate value of k_z (we concentrate on the fundamental mode, with $k_z = 2\pi/2L$). With the Fourier decomposition in z, the wave equation for the fast modes is the Klein-Gordon equation (Terradas et al. 2005a),

$$\frac{\partial^2 v_x}{\partial t^2} = v_{\rm A}^2\,\frac{\partial^2 v_x}{\partial x^2} - \omega_{\rm c}^2\,v_x, \tag{2}$$

where x is the coordinate in the direction normal to the magnetic field lines (see Fig. 1), v_x is the x-component of the velocity (v_y and v_z are both zero), $\omega_{\rm c} = k_z v_{\rm A}$ is the cut-off frequency and $v_{\rm A}$ is the Alvén speed,

$$v_{\rm A}(x) = \begin{cases} v_{\rm Ae} = \frac{B_0}{\sqrt{\mu\rho_{\rm e}}}, & \text{if } 0 \le |x| < d/2 - a, \\ v_{\rm Ai} = \frac{B_0}{\sqrt{\mu\rho_{\rm i}}}, & \text{if } |x \pm d/2| \le 2a, \\ v_{\rm Ae} = \frac{B_0}{\sqrt{\mu\rho_{\rm e}}}, & \text{if } |x| > d/2 + a. \end{cases} \tag{3}$$

3. Normal mode analysis

Before considering the time-dependent problem of perturbations about the equilibrium, we briefly describe the main oscillatory features of our two-slab model, given by the normal mode analysis. Normal mode solutions of Eq. (2) in a uniform medium have a dependence of the form $\mathrm{e}^{\mathrm{i}(\omega t - kx)}$ with $k^2 = \omega^2/v_{\rm A}^2 - k_z^2$. In the present structure, the velocity of normal modes has the form $v_x(x,t) = v_x(x)\,\mathrm{e}^{\mathrm{i}\omega t}$, with

$$v_x(x) = \begin{cases} A\,\mathrm{e}^{k_{\rm e}x}, & \text{if } x < -d/2 - a, \\ B_1\,\mathrm{e}^{-\mathrm{i}k_{\rm i}x} + B_2\,\mathrm{e}^{\mathrm{i}k_{\rm i}x}, & \text{if } -d/2 - a \le x \le -d/2 + a, \\ C_1\,\mathrm{e}^{k_{\rm e}x} + C_2\,\mathrm{e}^{-k_{\rm e}x}, & \text{if } |x| < d/2 - a, \\ D_1\,\mathrm{e}^{-\mathrm{i}k_{\rm i}x} + D_2\,\mathrm{e}^{\mathrm{i}k_{\rm i}x}, & \text{if } d/2 - a \le x \le d/2 + a, \\ E\,\mathrm{e}^{-k_{\rm e}x}, & \text{if } x > d/2 + a. \end{cases} \tag{4}$$

Here $k_{\rm e}$ and $k_{\rm i}$ are the external and internal wave numbers. The internal wave number is given by

$$k_{\rm i} = \sqrt{\frac{\omega^2}{v_{\rm Ai}^2} - k_z^2}. \tag{5}$$

Depending on the character of $k_{\rm e}$ and ω there are two types of solutions. Trapped modes are characterised by real $k_{\rm e}$ and ω, with

$$k_{\rm e} = \sqrt{k_z^2 - \frac{\omega^2}{v_{\rm Ae}^2}}. \tag{6}$$

Leaky modes are characterised by complex $k_{\rm e}$ and ω where Terradas et al. (2005b)

$$k_{\rm e} = -\sqrt{k_z^2 - \frac{\omega^2}{v_{\rm Ae}^2}}. \tag{7}$$

In addition, we consider the boundary conditions at the interfaces of the dense slabs and the coronal environment. Following Díaz (2004), these conditions reduce to the continuity of v_x and its x-derivative, $\frac{\partial v_x}{\partial x}$.

We then impose both boundary conditions on the four interfaces located at $x = -d/2 \pm a$ and $x = d/2 \pm a$, thus obtaining four equations for the velocity and four equations for its x-derivative. These equations form a homogeneous linear system of eight equations with eight unknowns, i.e. A, B_1, B_2, C_1, C_2, D_1, D_2, E in Eq. (4). For this system of equations to have a non-trivial solution, its determinant must be zero. This gives the dispersion relation, which appears as a product of two factors. One of these factors must vanish, which leaves us with the following expressions,

$$\left(k_{\rm e}^2 + k_{\rm i}^2\right)\tan(2\,a\,k_{\rm i}) - e^{(d-2\,a)\,k_{\rm e}}\left(\tan(a\,k_{\rm i}) - \frac{k_{\rm e}}{k_{\rm i}}\right) \times\left(\tan(a\,k_{\rm i}) + \frac{k_{\rm i}}{k_{\rm e}}\right) = 0, \tag{8}$$

or

$$\left(k_{\rm e}^2 + k_{\rm i}^2\right)\tan(2\,a\,k_{\rm i}) + e^{(d-2\,a)\,k_{\rm e}}\left(\tan(a\,k_{\rm i}) - \frac{k_{\rm e}}{k_{\rm i}}\right) \times\left(\tan(a\,k_{\rm i}) + \frac{k_{\rm i}}{k_{\rm e}}\right) = 0. \tag{9}$$

Moreover, the solutions of the homogeneous set of equations, i.e. the constants in Eq. (4), are the kernel of the matrix of the system.

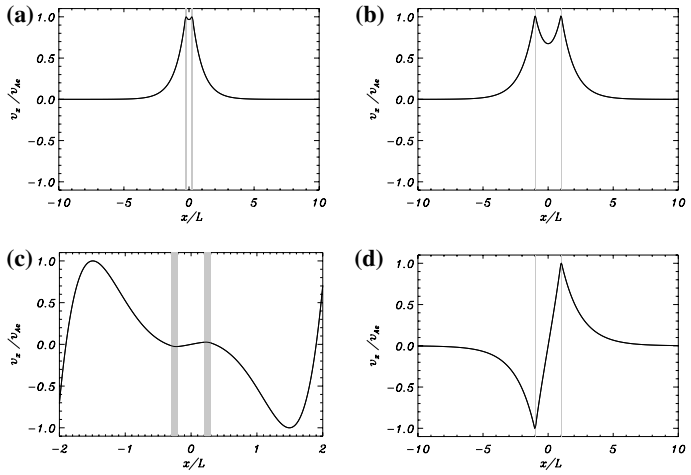

Fig. 2. Velocity profile, $v_x(x)$, for the fundamental symmetric mode (*upper row*) and the fundamental antisymmetric mode (*lower row*) for a slab half-width $a = 0.05L$ and a density enhancement $\rho_i/\rho_e = 3$. The left and right columns correspond to a distance between slabs $d = 0.5L$ and $d = 2L$, respectively. **a)** and **b)** show that the symmetric mode is trapped for the two separations, but **c)** and **d)** indicate that the antisymmetric mode becomes leaky for small distances. The shaded surface corresponds to the density enhancement of the slabs.

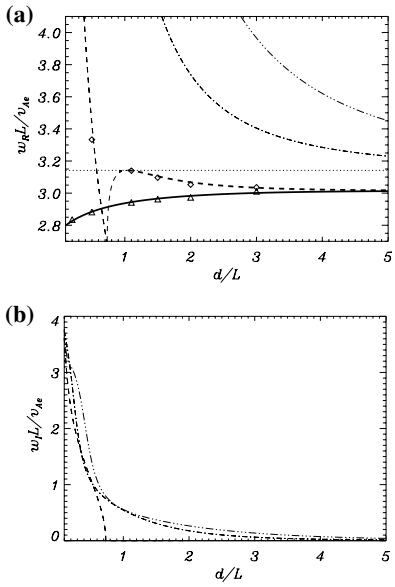

Fig. 3. a) Real part, ω_R, and **b)** imaginary part, ω_I, of the frequency as functions of the separation, d, for a density enhancement $\rho_i/\rho_e = 3$ and a half-width $a = 0.05L$. The line styles correspond to the fundamental symmetric mode (solid line), the fundamental antisymmetric mode (dashed line), the first symmetric harmonic (dot-dashed line) and the first antisymmetric harmonic (three-dot-dashed line). The dotted line is the external cut-off frequency, ω_{ce}. Thick curves represent trapped modes while thin lines correspond to leaky modes. $\omega_R L/v_{Ae}$ and $\omega_I L/v_{Ae}$ are normalised frequencies. In the top panel the calculated frequency from the time-dependent results for the symmetric (triangles) and antisymmetric (diamonds) modes is also represented.

Equations (8) and (9) indicate that there are two kinds of normal modes, whose spatial structure will be studied next. Solutions to Eq. (8) are symmetric with respect to $x = 0$ and both slabs move in phase (see Figs. 2a and b). On the other hand, solutions to Eq. (9) are antisymmetric with respect to $x = 0$ and both slabs move in antiphase (see Figs. 2c and d). In addition, Fig. 2 shows that normal modes can either be trapped (as in panels a, b and d) or leaky (as in panel c). Trapped modes attain their maximum amplitude in or near the slabs, but leaky modes present oscillations growing in amplitude as $x \to \infty$.

We solve the transcendental Eqs. (8) and (9) and calculate ω for different values of the slab separation, d, finding two types of curves (Fig. 3). Figures 3a and b correspond to the real and imaginary part of the frequency, that has been written as $\omega = \omega_R + i\omega_I$. Here we only represent the fundamental and first harmonic of the symmetric and antisymmetric modes. The frequency of trapped modes is real and smaller than the external cut-off frequency, $\omega_{ce} = \omega_c = k_z v_{Ae}$. Since $\omega_I = 0$ for trapped modes, these solutions correspond to standing oscillations of the system. Leaky modes have complex frequency with $\omega_I > 0$, so that they represent damped oscillations, the origin of the damping being that perturbations carry the energy away from the slabs. Figure 3 shows that the fundamental symmetric mode (solid line) is trapped for all distances. On the other hand, the fundamental antisymmetric mode (dashed line) starts as leaky for small values of d/L and, as d/L is increased, its curve crosses the external cut-off frequency, bifurcates and gives rise to two branches. At the bifurcation point the imaginary part of the frequency becomes zero (Fig. 3b) and the two branches have $\omega_I = 0$. Both branches are physically meaningless because they have $\omega_I = 0$ and k_e is real and negative, which implies an oscillatory solution in time with an exponential growth in space. For even larger separations between the slabs ($d/L \gtrsim 1$) the upper branch reaches the external cut-off and the mode becomes trapped (thick dashed line), becoming a physically relevant solution. All the harmonics (both symmetric and antisymmetric) have the same behaviour as the fundamental antisymmetric mode, although in the range of separations plotted in Fig. 3 they are leaky. From Fig. 3b we see that the damping time, $\tau = \omega_I^{-1}$, increases with the separation d.

The behaviour of solutions for small and large separations between slabs can be derived from Eqs. (8) and (9). For small separations, $d \gtrsim 2a$, we have $e^{(d-2a)k_e} \approx 1$ and from Eq. (8) we recover the sausage mode dispersion relation for one slab,

$$\tan(2ak_i) = -\frac{k_i}{k_e}, \tag{10}$$

and from Eq. (9) the kink mode dispersion relation for one slab,

$$\tan(2ak_i) = \frac{k_e}{k_i}. \tag{11}$$

These formulas are identical to those in Edwin & Roberts (1982) and Terradas et al. (2005b), although a is now replaced by $2a$. Therefore, for the minimum separation between slabs, $d = 2a$, the system of two slabs is equivalent to a single slab but with half width $2a$. We also see that the symmetric mode tends to the kink mode for $d \to 2a$ and the antisymmetric mode tends to the sausage mode. Hence, we expect a gradual transition from the solutions of one slab to those of a system of two slab as the separation is increased.

For a very large separation between slabs, $e^{(d-2a)k_e} \to \infty$, both Eqs. (8) and (9) lead to

$$\left(\tan(a\,k_i) - \frac{k_e}{k_i}\right)\left(\tan(a\,k_i) + \frac{k_i}{k_e}\right) = 0. \tag{12}$$

This is the dispersion relation of one slab. This is the expected behaviour, too, since for large separations the interaction between both slabs is negligible and they behave as independent loops.

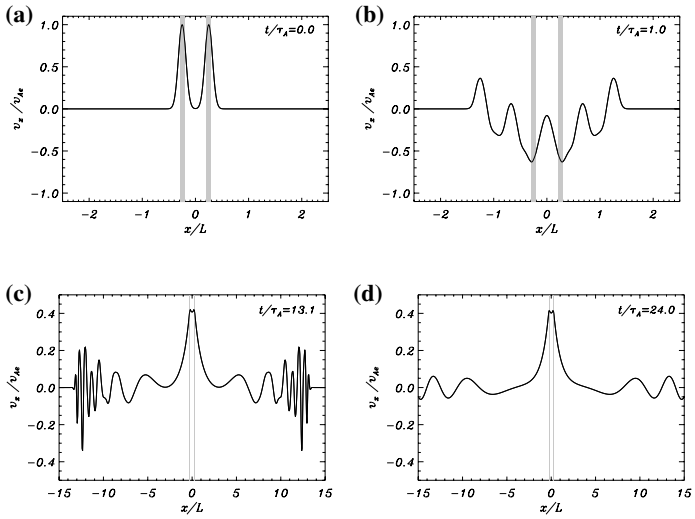

Fig. 4. Time-evolution of the velocity, v_x, for a distance between slabs $d = 0.5L$ and a symmetric initial impulse.

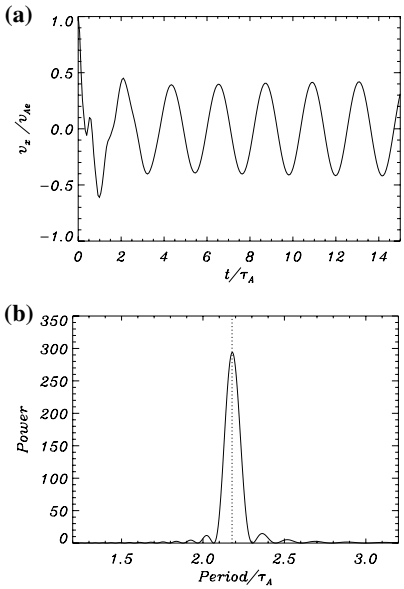

Fig. 5. a) Measured velocity at the centre of the right slab, $x = d/2$, for the symmetric initial perturbation of Fig. 4. After a short transient the system oscillates in a trapped mode, with period close to $2\tau_{\rm A}$, and the oscillatory amplitude remains unchanged. **b)** As expected, the periodogram of the signal in **a)** features a large power peak at a period around $2\tau_{\rm A}$. There is an excellent agreement between the period of this peak and the period of the normal mode obtained from Eq. (8) (dotted line). The periodogram lacks other power peaks.

4. Time-dependent analysis: numerical simulations

Normal modes provide with information about the oscillatory state and parameters of the system, but coronal oscillations are often produced by an impulsive event and time dependent simulations are more appropriate to describe the evolution of the system. In the case of a single slab (Terradas et al. 2005b) an impulsive disturbance leads, after a time of the order of the Alfvén transit time across the slab, to a distribution of its energy into one or more normal modes. The question that arises is how this picture will be modified for a two-slab structure: after an impulsive event, does the system oscillate in a normal mode (or a sum of some normal modes) or do the modes of a single slab appear?

To study the effect of an arbitrary initial perturbation we consider the system of two slabs with a typical density enhancement ($\rho_{\rm i}/\rho_{\rm e} = 3$), a typical slab half-width ($a = 0.05L$) and we excite perturbations with different velocity profiles.

To solve Eq. (2) numerically the code *PDE2D*, (Sewell 2005), based on finite elements, has been used. The code, which gives a numerical approximation to $v_x(x,t)$, makes use of a second order implicit Crank-Nicholson method with adaptive time step control. Since we consider a finite numerical domain, reflections at the domain boundaries may affect the dynamics of the system of slabs. We have solved this problem by locating the edges of the numerical domain far from the two slabs. Given that the size of the domain is much larger than the loop thickness, a non-uniform grid with 4000 grid points in the full domain, 45 of them located inside each slab ($|x \pm d/2| \leq a$), has been used. In addition, we have made sure that the artificial diffusion introduced by the numerical scheme is small enough. This is a critical point since the artificial damping can be larger than the physical damping, in our case arising from energy leakage, and may lead to the wrong interpretation of the results. We have performed different simulations by increasing the number of grid points and have found that the solutions converge, which is an indication that numerical diffusion does not affect considerably the results. In addition, we have checked that the same results are obtained by solving the initial-value problem with a standard explicit method based on finite differences.

The initial condition is the sum of two Gaussian profiles centred in each of the slabs,

$$v_x(x, t = 0) = \left\{ A \exp\left[\left(\frac{x - d/2}{\Delta}\right)^2\right] + B \exp\left[\left(\frac{x + d/2}{\Delta}\right)^2\right]\right\}, \quad (13)$$

where Δ is the width of the Gaussian function and A and B are the amplitudes of the right and left Gaussian pulses, respectively. Firstly, we generate two types of initial conditions, namely a symmetric initial pulse ($A = B = 1$) and an antisymmetric initial pulse ($A = -B = 1$). Later, we excite the system with an individual pulse with $A = 1$ and $B = 0$. In all the numerical simulations performed, the width of the initial pulses is $\Delta = 0.1L$.

4.1. Symmetric or antisymmetric excitation

Let us start with the symmetric initial condition and a separation between slabs $d = 0.5L$. To see which normal modes can be excited, we only need to care about the symmetric ones, since the antisymmetric modes are not excited because their symmetry is opposite to that of the initial perturbation. So we inspect the dispersion diagram (Fig. 3) and see that for $d = 0.5L$ there is only a symmetric trapped mode (the fundamental symmetric mode) and infinite leaky symmetric modes (of which only one is shown in this plot). The results of the simulation are displayed in Fig. 4, where we have plotted the velocity, v_x, as a function of x for different times (t is given in units of the external Alfvén transit time, $\tau_{\rm A} = L/v_{\rm Ae}$). The initial perturbation produces travelling disturbances to the left and right and these disturbances show some dispersion as they propagate: short wavelengths are at the front and long wavelengths at the back of the travelling disturbances (Figs. 4c and d). A comparison of Figs. 2a and 4d in the range $-5 \leq x \leq 5$ indicates that, for long times, the system settles down into the trapped mode. To gain more insight

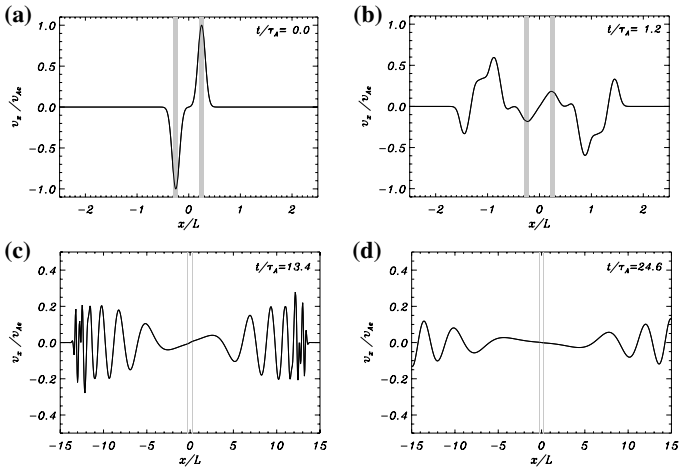

Fig. 6. Time-evolution of the velocity, v_x, for a distance between slabs $d = 0.5L$ and an antisymmetric initial impulse.

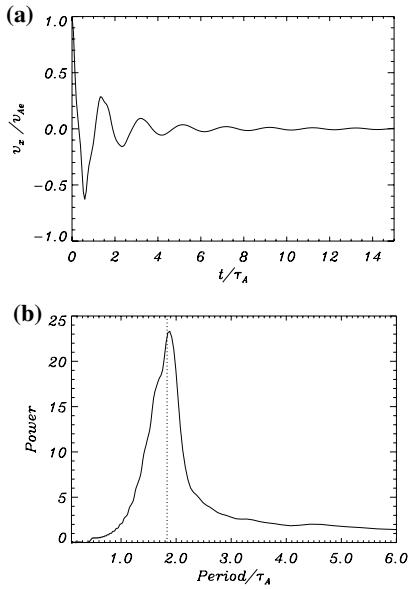

Fig. 7. a) Measured velocity at the centre of the right slab, $x = d/2$, for the antisymmetric initial perturbation of Fig. 6. After a short transient the system oscillates in a leaky mode and so the perturbation attenuates exponentially. **b)** The periodogram of the signal in **a)** has a power peak whose period is in excellent agreement with that of the normal mode obtained from Eq. (9) (dotted line). The periodogram lacks other power peaks.

into the time evolution we plot the velocity at the centre of the right slab (at $x = d/2$) in Fig. 5a. In this figure we see clearly two phases, a transient (for $0 \leq t/\tau_A \lesssim 3$) and an oscillatory phase (for $t/\tau_A \gtrsim 3$). The transient is produced by two effects: firstly, perturbations reflect and refract at the two slabs until the energy contained in the initial impulse is transferred into the normal modes. This phase has a duration, which we call the relaxation time, of the order of a few times the Alfvén travel time between the two slabs, i.e. a few times $0.5\tau_A$; secondly, the excited leaky modes carry their energy towards $x \to \pm\infty$ and so decay in a time of the order of τ_I. In Terradas et al. (2005b) this phase was called the impulsive leaky phase. From Fig. 3b we see that $\tau_I/\tau_A \simeq 1$ for the first leaky harmonic, which means that this mode damps out in a time comparable to the relaxation time. The very short duration of this and all other leaky modes makes them practically undetectable in Fig. 5a. Further confirmation of this interpretation of Fig. 5a is given in its power spectrum (Fig. 5b), which displays a single power peak whose frequency exactly matches that of the trapped symmetric mode, while the power at the frequencies of leaky modes is negligible. As a conclusion, the trapped fundamental symmetric mode is excited in this simulation and there is a good agreement in the frequency and velocity profile with the normal mode results. If leaky modes are excited, they cannot be detected because of their very rapid damping.

Next, we perturb the same system with an antisymmetric initial condition, so now the antisymmetric normal modes are excited. The results of the simulation, which again show the propagation of perturbations in both directions along the x-axis, are displayed in Fig. 6. In this case the amplitude of the oscillations in both slabs decrease in time because all antisymmetric modes are leaky for the selected separation between slabs ($d/L = 0.5$). In Fig. 7a the velocity measured in the centre of the right slab, $x = d/2$, is plotted. After the relaxation time, which again is of the order of $3\tau_A$, the signal is an attenuated oscillation, as expected for leaky modes. In Fig. 7b we see the periodogram of this signal, where the dashed line gives the theoretical frequency of the fundamental leaky antisymmetric mode (from Fig. 3) and as in the previous case coincides with the peak of the power spectrum. Nevertheless, now the power peak is broad due to the exponential attenuation of the signal. Regarding the spatial velocity profile, it is not easy to compare the results of the simulation with those of the normal mode analysis, but still Figs. 6c and d bear some resemblance with Fig. 2c. We conclude that the considered antisymmetric disturbance mostly excites the fundamental antisymmetric leaky mode.

We next repeat this analysis for different slab separations and obtain an estimation of the real part of the frequency of the normal mode, ω_R, from the power spectrum of the simulations. With these data we have superimposed in Fig. 3a, the value of ω_R calculated from the numerical simulations (see triangles and diamonds) on top of the theoretical dispersion diagram. The agreement is outstanding for all values of d/L, so we conclude that when the system is excited with a symmetric or antisymmetric initial condition, it later oscillates in a normal mode predicted by the theory. As a corollary, the system acquires a collective oscillation, given by a normal mode, and does not oscillate with the modes of an individual slab.

4.2. Arbitrary excitation

Now, the system is excited using an initial condition with no particular symmetry about $x = 0$. The initial condition that we consider is a Gaussian pulse centred in the right slab. This initial pulse is given by Eq. (13) with $A = 1$, $B = 0$ and, therefore, can be decomposed into the sum of a symmetric and an antisymmetric excitation. Since Eq. (2) is linear, we expect that this kind of initial disturbance will give rise to a superposition of the solutions arising from the corresponding symmetric and antisymmetric excitations. In this section we consider the slab separations $d = 0.5L$ and $d = 2L$.

Firstly, we consider the case $d = 0.5L$ (Fig. 8), which implies that the initial condition (Fig. 8a) is half the sum of the symmetric and antisymmetric initial conditions of Sect. 4.1. During the initial stages of the temporal evolution (Figs. 8b and c) v_x has no definite symmetry with respect to $x = 0$ because the solution is the sum of the symmetric and antisymmetric modes of Sect. 4.1. Let us recall that these modes are the fundamental symmetric and the fundamental antisymmetric, which are trapped and

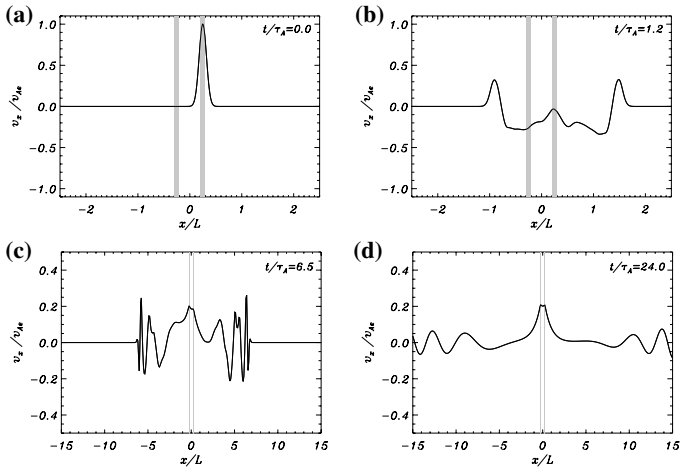

Fig. 8. Time-evolution of v_x for $d = 0.5L$ and a non-symmetric initial excitation.

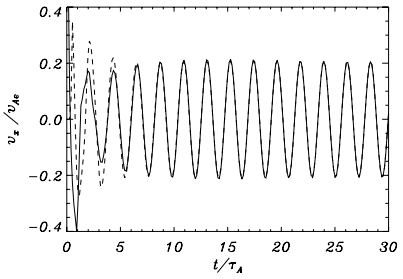

Fig. 9. v_x measured at the centres of the slabs for the simulation shown in Fig. 8. The solid and dashed lines correspond to the right and left slabs, respectively.

leaky, respectively. As a consequence, after some time (Fig. 8d) the antisymmetric mode amplitude is negligible in the vicinity of the slabs and the system oscillates in a symmetric manner. In Fig. 9 the time dependence of the velocity, v_x, is plotted in both slab centres. Because of the superposition of the antisymmetric leaky mode and the symmetric trapped mode both slabs oscillate with different phases and amplitudes until $t \simeq 10\tau_{\rm A}$. Then, according to Fig. 7a, the antisymmetric perturbation extinguishes and the two slabs oscillate in phase. The periodogram of the two curves in this plot coincides with that Fig. 5b because the leaky mode is a very short duration signal and so its contribution to the periodogram is very small. In addition, Fig. 9 gives us a way of recovering the signals in Figs. 5a and 7a. By summing the signals in Fig. 9 the contribution of the antisymmetric modes vanishes because they have the same amplitude and opposite sign in the slab centres, so we are left with the symmetric mode, i.e. with Fig. 5a. In the same manner, the difference of the signals in Fig. 9 leads to Fig. 7a. We thus conclude that the initial condition excites the symmetric and antisymmetric modes, as expected, and that the system oscillates in its collective modes and not in the modes of a single slab.

Secondly, we perturb the system with the same initial condition but now the distance between the slab centres is $d = 2L$. As can be appreciated in Fig. 3, this choice of the slab separation results in the fundamental antisymmetric mode becoming trapped. The evolution of the system is again presented for different times (Fig. 10) and, although after some time the two slabs seem to move in phase (Fig. 10b), in a later stage the right slab has given all its energy to the left slab and so is motionless (Fig. 10c). At an even later time (Fig. 10d) the picture is just the

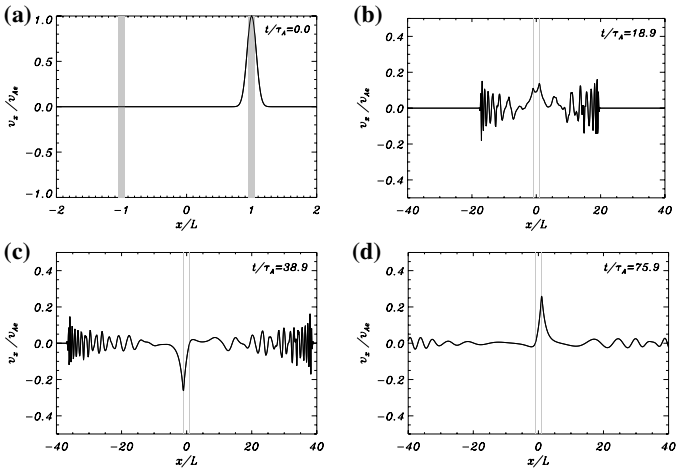

Fig. 10. Time evolution of v_x for $d = 2L$ and a non-symmetric initial disturbance. Note the interchange of energy between the two slabs in the last two frames.

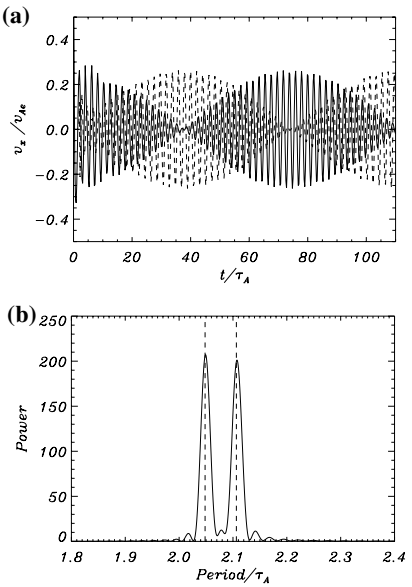

Fig. 11. a) v_x measured at the centre of the slabs for the simulation shown in Fig. 10. The solid and dashed lines correspond to the right and left slabs, respectively. **b)** Power spectrum of the previous signal (solid line). The two vertical dashed lines indicate the periods of the fundamental antisymmetric mode (at $2.04821\tau_{\rm A}$) and the fundamental symmetric mode ($2.10633\tau_{\rm A}$).

opposite, with the left slab fixed and the right slab in motion. Hence, the two slabs are continously exchanging energy and the transition between the states depicted in Figs. 10c and d takes place through a situation similar to that in Fig. 10b, where both slabs are oscillating. This behaviour is repeated periodically. This phenomenon is more clearly represented in Fig. 11a, where the velocity, v_x, is plotted at the centre of both slabs. Contrary to the behaviour in the stationary regime for symmetric or antisymmetric initial perturbations (Figs. 5a and 7a), the oscillations do not attain a constant amplitude, but they instead display a sinusoidal modulation. This is a well known collective beating phenomenon, like, for instance, that of two weakly coupled oscillators. It is due to the simultaneous excitation of the symmetric and antisymmetric modes with alike frequencies. These frequencies are recovered from the power spectrum of the velocity at the centre of right slab (Fig. 11b), which shows two power peaks

with periods almost identical to those of the fundamental antisymmetric mode ($2.04821\tau_A$) and the fundamental symmetric mode ($2.10633\tau_A$). This match between the frequency of the normal modes and the oscillations in the numerical simulation is also evident in Fig. 3a. Both peaks in the power spectrum have similar height, which allows us to conclude that the two normal modes have been excited with similar amplitude.

In fact, from Fig. 3 we see that there exists a range of slab separations where both trapped modes, i.e. the fundamental symmetric and antisymmetric, coexist and possess very close frequencies. In this range of separations, which goes from $d \approx 1.04L$ to infinity, the beating appears when non-symmetric initial disturbances are applied. Hereafter we refer to this range of d as the band of beating and to the separation where the band starts as the minimum distance of beating ($d_{\min}$). Then, our analysis yields $d_{\min} \simeq 1.04L$ for $a/L = 0.05$ and $\rho_i/\rho_e = 3$. In Sect. 5.1, we shall study the beating properties for other density ratios and will show that this band extends to smaller separations.

5. Analytical study of beating

For a slab separation in the beating band the system oscillates in a superposition of the trapped symmetric and antisymmetric modes. Then, in the stationary state, the system behaves as

$$v_x(x,t) = \alpha_s f_s(x)\cos(\omega_s t + \phi_0) + \alpha_a f_a(x)\cos(\omega_a t), \quad (14)$$

where the subscripts s and a refer to the symmetric and antisymmetrical modes, respectively. The spatial functions $f_s(x)$ and $f_a(x)$ are the corresponding eigenfunctions, for instance the velocity profiles of Figs. 2b and d (for $d/L = 2$). The parameters α_s and α_a are scaling factors that correspond to the amplitude of the normal modes.

We define

$$\Omega_+ = \frac{\omega_a + \omega_s}{2}, \quad (15)$$

$$\Omega_- = \frac{\omega_a - \omega_s}{2}, \quad (16)$$

and

$$f_1(x) = \alpha_a f_a(x) + \alpha_s f_s(x), \quad (17)$$

$$f_2(x) = \alpha_a f_a(x) - \alpha_s f_s(x). \quad (18)$$

After some algebra we find

$$v_x(x,t) = f_1(x)\cos(\Omega_+ t + \phi_0/2)\cos(\Omega_- t - \phi_0/2) - f_2(x)\sin(\Omega_+ t + \phi_0/2)\sin(\Omega_- t - \phi_0/2). \quad (19)$$

We next consider

$$v_{x1}(x,t) = f_1(x)\cos(\Omega_+ t + \phi_0/2)\cos(\Omega_- t - \phi_0/2), \quad (20)$$

$$v_{x2}(x,t) = -f_2(x)\sin(\Omega_+ t + \phi_0/2)\sin(\Omega_- t - \phi_0/2), \quad (21)$$

so that Eq. (20) can be written as

$$v_x(x,t) = v_{x1}(x,t) + v_{x2}(x,t). \quad (22)$$

We now focus on the situation that led to beating in Sect. 4.2, that is, a system with $d/L = 2$ and the two trapped modes excited with identical amplitude. Then $f_1(x)$ and $f_2(x)$ (see Fig. 12) come from the eigenfunctions $f_s(x)$ and $f_a(x)$ of Figs. 2b and d and the mode amplitudes are identical, so we take $\alpha_s = \alpha_a = 1$. In Fig. 12 we see that $f_1(x)$ and $f_2(x)$ are peaked functions around the right and left slabs, respectively. Therefore, the function $v_{x1}(x,t)$, for example, is also relevant in the neighbourhood

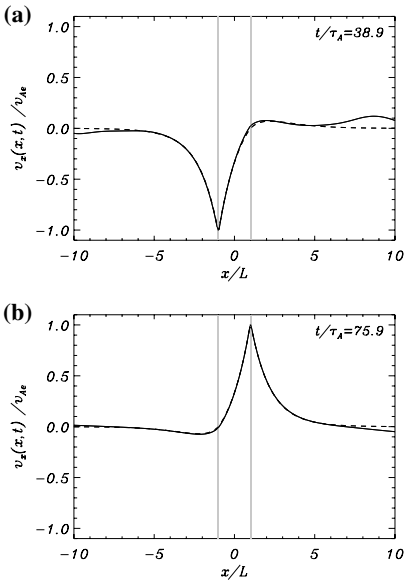

Fig. 12. The solid lines are a rescaled close-up view of Figs. 10d and c, respectively. The dashed lines correspond to $f_1(x)$ and $f_2(x)$, respectively. The analytical approximation then reproduces the velocity profile obtained in the time-dependent simulation when a substantial amount of energy is concentrated in a single slab. The difference among both curves to the right and left of the slabs arises from the system not having reached the stationary state. For greater times the difference becomes smaller.

of the right slab and is negligible in the vicinity of the left one (the opposite applies to $v_{x2}(x,t)$). This confers an intrinsic meaning to these functions that, although not directly measurable, reproduce some features of the numerical simulations. For example, at $t_1 = 38.9\tau_A$ in the numerical simulation (Fig. 10c) the left slab reaches its maximum velocity and so the main contribution to the analytical approximation of the velocity (Eq. (22)) comes through $v_{x2}(x,t_1)$, i.e. through $-f_2(x)$. For this reason, the spatial distribution of v_x in Fig. 10c is very well reproduced by $-f_2(x)$, as can be seen in Fig. 12b. Moreover, Fig. 12a shows a similar agreement for the left slab at $t_2 = 75.9\tau_A$.

Given the spatial structure of v_{x1} and v_{x2}, the velocity in the centre of the right and left slabs obtained in the numerical simulations should be similar to $v_{x1}(x = d/2, t)$ and $v_{x2}(x = -d/2, t)$, respectively, so we have plotted these two functions together with their numerical counterparts (Fig. 13). During the transient phase, the analytical approximation differs from the time-dependent results, but once the stationary state is reached (around $t = 12\,\tau_A$) the fitting is very good. The small difference between the two solutions in the stationary phase is caused by the slight amplitude difference of the two normal modes in the numerical simulation (see Fig. 11b).

The beating oscillatory curve is a sinusoidal function multiplied by a sinusoidal envelope whose period (the beating period) is

$$T_{\text{beating}} = \frac{2\pi}{\Omega_-} = \frac{4\pi}{\omega_a - \omega_s}. \quad (23)$$

In addition, the period of oscillation of the system is

$$T = \frac{2\pi}{\Omega_+} = \frac{4\pi}{\omega_a + \omega_s}. \quad (24)$$

From the agreement found between the numerical simulations and the behaviour of v_{x1} and v_{x2} (see Fig. 13) it is clear that

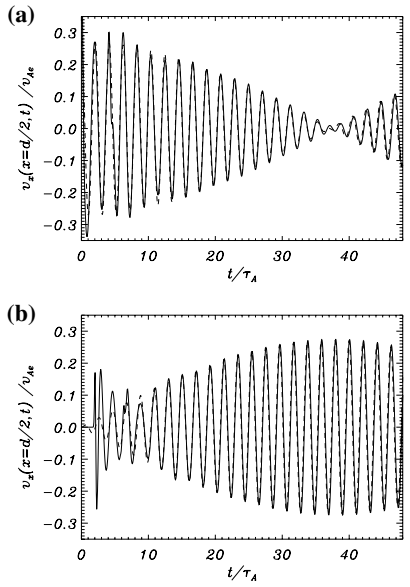

Fig. 13. a) Superposition of v_x measured at the centre of the right slab from the time-dependent numerical simulation (solid line) and the analytical approximation (dashed line). **b)** The same for the left slab.

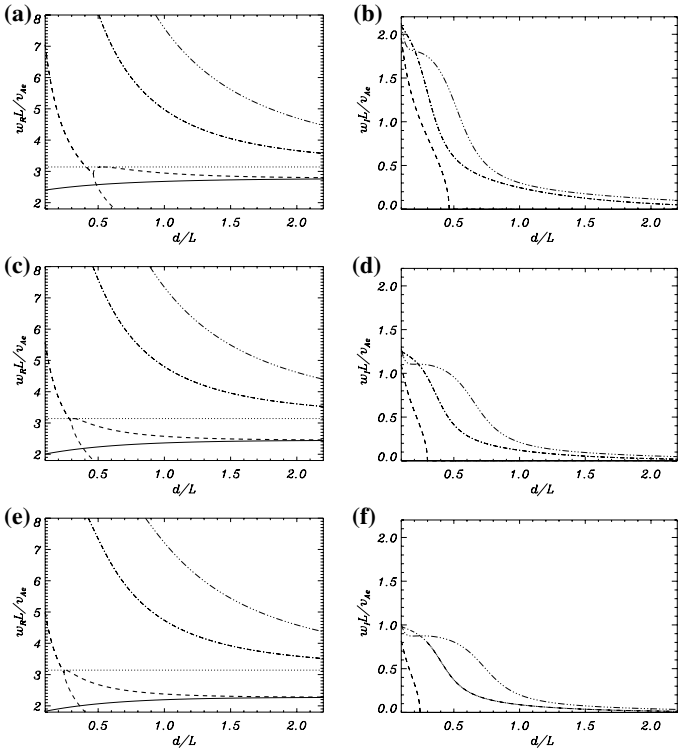

Fig. 14. Plots of ω_R (*left column*) and ω_I (*right column*) as functions of the slab separation for different values of the density enhancement, ρ_i/ρ_e. **a)** and **b)** $\rho_i/\rho_e = 5$; **c)** and **d)** $\rho_i/\rho_e = 8$; **e)** and **f)** $\rho_i/\rho_e = 10$.

the beating period and oscillation period calculated from these simulations is in perfect agreement with Eqs. (23) and (24) respectively.

In addition, it is useful to define the number of oscillations within a pulsation period, or beating factor (b_f),

$$b_f \equiv \frac{T_{\rm beating}}{T} = \frac{\Omega_+}{\Omega_-} = \frac{\omega_a + \omega_s}{\omega_a - \omega_s}. \qquad (25)$$

This factor is the number of peaks in a beating period. Small beating factors indicate strong beating behaviour. The beating factor is a good parameter to assess the beating phenomenon since it is easily measurable from the time-dependent results. In our example of Fig. 11b, the number of peaks in a full beating period is approximately 71; this coincides with the theoretical beating factor given by the last expression, $b_f = 71.5$.

5.1. Parameter dependence of the beating

We investigate the beating properties of two identical slabs with different separations and density contrasts (the slabs width is held fixed and given by $a/L = 0.05$). In the previous section we have seen that the dispersion relation allows us to extract information about the beating with the help of Eqs. (23), (24) and (25). For this reason we start plotting the real and imaginary parts of the frequency as functions of d for different values of ρ_i/ρ_e (see Fig. 14). In these plots we can appreciate that the minimum distance of beating (i.e. the slab separation for which the fundamental antisymmetric mode transforms from leaky into trapped) decreases as the density ratio increases. This means that denser slabs can display beating for smaller separations. The oscillatory period obtained from Eq. (24) is plotted in Fig. 15a. For all the considered values of ρ_i/ρ_e, the oscillatory period is more or less independent from the slab separation when this quantity is larger than the length of the loops. Nevertheless, for $d < L$ (and for sufficiently high values of the density contrast, like for example $\rho_i/\rho_e = 8$ or 10) the oscillatory period decreases as the separation is reduced.

Two other parameters worth studying are the beating period, $T_{\rm beating}$, and the beating factor, b_f, extracted from the dispersion relation data and Eqs. (23) and (25). These parameters are plotted in Figs. 15b and c, respectively. We see that the beating period grows to infinity with d/L which is the expected behaviour of two slabs that tend to oscillate independently. On the other hand, we see that for small slab separations b_f becomes rather small, implying that each beating period contains only a few oscillatory periods. In particular, we find that slabs with high density contrast can show strong beating for small distances in comparison with slabs with small density contrasts.

6. Conclusions

We have studied the main features of a simple two-slab configuration (without gravity and curvature). Firstly, we have analysed in detail the normal modes of the system. We have derived analytical expressions for the dispersion relation and have found, in agreement with the results of Díaz et al. (2005), that the symmetric mode is the only trapped mode for any distance between the slabs. On the other hand, the antisymmetric mode is leaky for small slab separations, but there exists a wide range of slab separations (larger than the critical distance) where both trapped modes, i.e. the fundamental symmetric and antisymmetric, coexist and possess very close frequencies. Thus, trapped and/or leaky modes are excited according to the ratio d/L, but also according to the shape of the initial perturbation. It is then expected that initial disturbances with odd parity with respect to the centre of the system excite antisymmetric modes, whereas even disturbances lead to the excitation of symmetric modes.

Secondly, we have studied the temporal evolution of symmetric, antisymmetric and arbitrary excitations for a typical coronal loop with $a/L = 0.05$ and $\rho_i/\rho_e = 3$ and different slab separations. We have found that for symmetric disturbances and after a short transient all that remains is the undamped trapped

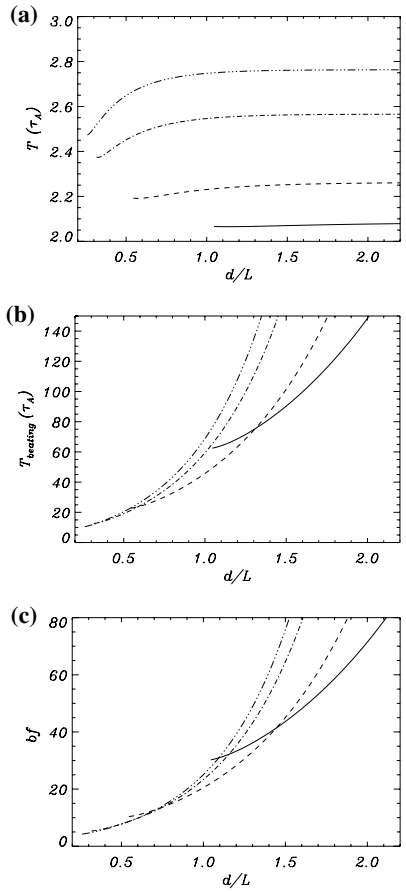

Fig. 15. a) Oscillatory period, **b)** beating period and **c)** beating factor, for the density contrasts $\rho_i/\rho_e = 3$ (solid line), $\rho_i/\rho_e = 5$ (dashed line), $\rho_i/\rho_e = 8$ (dot-dashed line) and $\rho_i/\rho_e = 10$ (three-dot-dashed line). Note that the curves start at the slab separation for which the fundamental antisymmetric mode transforms from leaky into trapped.

mode, with energy confined to both slabs. On the other hand, since there are no trapped antisymmetric modes for slab separations smaller that $d_{\min}$, an antisymmetric-like initial disturbance can only deposit energy in the leaky antisymmetric modes. The excitation of the fundamental antisymmetrical trapped mode is only possible for $d > d_{\min}$.

An arbitrary excitation in the regime $d > d_{\min}$ leads to the simultaneous excitation of the symmetric and antisymmetric modes. Since their frequencies are quite similar the oscillations do not attain a constant amplitude and show a sinusoidal modulation. This is a well known collective beating phenomenon which is completely equivalent to the behaviour of two weakly coupled oscillators. The frequency of oscillation of the system is $\frac{\omega_a+\omega_s}{2}$ with an envelope frequency or beating frequency $\frac{\omega_a-\omega_s}{2}$, where ω_a and ω_s are the antisymmetric and symmetric normal mode frequencies, respectively. The beating is the result of the continuous exchange of energy between the two slabs. We have also shown that slabs with high density contrast can show strong beating for small distances in comparison with slabs with small density contrasts.

It is important to remark that for moderate slab separations and any type of initial excitation, the system acquires a collective motion and does not oscillate with the modes of an individual slab. For this reason, and specially in coronal arcades, formed by ensembles of loops, it seems much more appropriate to describe the oscillations in terms of collective motions instead of individual loop oscillations. Nevertheless, since our model is too simple, it has no sense to perform a quantitative comparison with the observations of loop oscillations in coronal arcades. However, it is worth noticing that the most clear example of such kind of oscillations (see Verwichte et al. 2004) suggests that initially some loops of the arcade oscillate in phase while at later times the motions are in antiphase. This can be an indication of beating phenomenon as the result of the collective oscillation of some of the loops. Unfortunately, it is not possible to extract more conclusions since the amplitude of the oscillations is quickly damped and only a few periods are observed. Additional observations of oscillations in coronal arcades will be very useful.

Finally, in order to have a more realistic model additional effects such as gravity, gas pressure and curvature need to be included. However, one of the most significant improvements to the model is to consider two cylindrical loops instead of Cartesian slabs. Since the eigenfunction in cylindrical tubes are much more confined than in slabs, the interaction between the tubes will be in general smaller and the beating time will be much longer. In addition, instead of the two modes of the Cartesian slab (symmetric and antisymmetric), now the system will have four different modes of oscillation. Two of these modes will be symmetric while the other two will be antisymmetric in the x and y-directions. The normal mode analysis of this configuration will be the subject of a future work.

Acknowledgements. M. Luna thanks to Spanish Ministry of Education and Science for an FPI grant, which is partially supported by the European Social Fund. In addition, J. Terradas thanks the Spanish Ministry of Education and Science for the funding provided under a Juan de la Cierva fellowship. The authors acknowledge the Spanish Ministry of Science and Technology and the Conselleria d'Economia, Hisenda i Innovació of the Government of the Balearic Islands for the funding provided under grants AYA2003-00123 and PRIB-2004-10145, respectively.

References

Aschwanden, M. J., Fletcher, L., Schrijver, C. J., & Alexander, D. 1999, ApJ, 520, 880
Aschwanden, M. J., De Pontieu, B., Schrijver, C. J., & Title, A. M. 2002, Sol. Phys., 206, 99
Berton, R., & Heyvaerts, J. 1987, Sol. Phys., 109, 201
Bogdan, T. J., & Fox, D. C. 1991, ApJ, 379, 758
Cally, P. S. 1986, Sol. Phys., 103, 277
Cally, P. S. 2003, Sol. Phys., 217, 95
Díaz, A. J. 2004, Ph.D. Thesis, Universitat de les Illes Balears, Spain
Díaz, A. J., Oliver, R., & Ballester, J. L. 2005, A&A, 440, 1167
Edwin, P. M., & Roberts, B. 1982, Sol. Phys., 79, 239
Edwin, P. M., & Roberts, B. 1983, Sol. Phys., 88, 179
Keppens, R., Bogdan, T. J., & Goossens, M. 1994, 436, 372
Murawski, K. 1993, Acta Astron., 43, 2, 161
Murawski, K., & Roberts, B. 1994, Sol. Phys., 151, 305
Schrijver, C. J., Aschwanden, M. J., & Title, A. M. 2002, Sol. Phys., 206, 69
Sewell, G. 2005, The Numerical Solution of Ordinary and Partial Differential Equations (Wiley-Interscience)
Spruit, H. C. 1982, Sol. Phys., 75, 3
Terradas, J., Oliver, R., & Ballester, J. L. 2005a, ApJ, 618, L149
Terradas, J., Oliver, R., & Ballester, J. L. 2005b, A&A, 441, 371
Verwichte, E., Nakariakov, V. M., Ofman, L., & Deluca, E. E. 2004, Sol. Phys., 223, 77